Destabilization of the PCNA trimer mediated by its interaction with the NEIL1 DNA glycosylase

Aishwarya Prakash[1,*], Kedar Moharana[2], Susan S. Wallace[2] and Sylvie Doublié[2,*]

[1]Department of Oncologic Sciences, Mitchell Cancer Institute, University of South Alabama, 1660 Springhill Avenue, Mobile, AL 36604-1405, USA and [2]Department of Microbiology and Molecular Genetics, The Markey Center for Molecular Genetics, University of Vermont, Stafford Hall, 95 Carrigan Drive, Burlington, VT 05405-0068, USA

ABSTRACT

The base excision repair (BER) pathway repairs oxidized lesions in the DNA that result from reactive oxygen species generated in cells. If left unrepaired, these damaged DNA bases can disrupt cellular processes such as replication. NEIL1 is one of the 11 human DNA glycosylases that catalyze the first step of the BER pathway, i.e. recognition and excision of DNA lesions. NEIL1 interacts with essential replication proteins such as the ring-shaped homotrimeric proliferating cellular nuclear antigen (PCNA). We isolated a complex formed between NEIL1 and PCNA (±DNA) using size exclusion chromatography (SEC). This interaction was confirmed using native gel electrophoresis and mass spectrometry. Stokes radii measured by SEC hinted that PCNA in complex with NEIL1 (±DNA) was no longer a trimer. Height measurements and images obtained by atomic force microscopy also demonstrated the dissociation of the PCNA homotrimer in the presence of NEIL1 and DNA, while small-angle X-ray scattering analysis confirmed the NEIL1 mediated PCNA trimer dissociation and formation of a 1:1:1 NEIL1-DNA-PCNA(monomer) complex. Furthermore, *ab initio* shape reconstruction provides insights into the solution structure of this previously unreported complex. Together, these data point to a potential mechanistic switch between replication and BER.

INTRODUCTION

Reactive oxygen species (ROS) generated by external environmental factors and endogenous agents during processes of cellular metabolism cause damage to DNA (1,2). Oxidized DNA bases resulting from ROS are produced at the rate of 20 000–40 000 per human cell per day and if left unrepaired can lead to various outcomes including the build-up of harmful mutations, replication stress, changes in epigenetic regulation and in some instances can lead to apoptosis (3–7). The highly-conserved base excision repair (BER) pathway is involved in the repair of oxidized DNA bases where the first step of repair is catalyzed by a specific DNA glycosylase (5,8–11). There are 11 mammalian DNA glycosylases of which the Nei-like NEIL1, 2 and 3 enzymes belong to the Fpg/Nei family named after the bacterial prototypes formamidopyrimidine DNA glycosylase (Fpg) and endonuclease VIII (Nei) (12–15). The NEIL enzymes are bifunctional in that they are able to cleave the N-glycosidic bond (glycosylase activity) as well as the DNA backbone 3′ to the lesion (lyase activity). NEIL1, NEIL2 and NEIL3 excise pyrimidine-derived lesions as well as purine-derived lesions such as formamidopyrimidines and hydantoin lesions (spiroiminodihydantoin and guanidinohydantoin) (16–19). Despite these overlapping lesion preferences, the NEIL enzymes differ in their ability to cleave lesions from specific DNA secondary structures. For example, NEIL1 can excise lesions from bubble, fork and duplex DNA, whereas NEIL2 prefers lesions in single-stranded DNA (ssDNA), and bubble structures, while studies performed with mouse NEIL3 indicate its ability to excise lesions present in ssDNA, duplex DNA and G-quadruplex structures (17,20,21). Of the three NEIL enzymes, it appears as though the expression of NEIL3 fluctuates throughout the cell cycle with induction of expression seen during early S-phase and highest expression levels observed in G2 whereas expression of NEIL2 appears to be cell-cycle independent (22–24). For NEIL1, conflicting lines of evidence indicate that it is either not cell-cycle regulated as seen in studies using synchronized HeLa cells or is upregulated during S-phase as observed with serum-starved fibroblasts (23,25,26). The latter points toward a role for NEIL1 during DNA replication where it assumes the function of a 'cowcatcher' ahead of the replication machinery (25–27). To further support this hypothesis, NEIL1 was observed to co-localize with proteins involved in replication via a disordered region in the C-terminal tail of the enzyme (26). Some of these interacting partners include replication protein A, flap structure-specific endonu-

*To whom correspondence should be addressed. Tel: +251 410 4915; Email: aprakash@health.southalabama.edu
Correspondence may also be addressed to Sylvie Doublié. Tel: +1 802 656 9531; Fax: +1 802 656 8749; Email: Sylvie.Doublie@uvm.edu

cleave 1 (FEN1), polymerase delta, replication factor C and proliferating cell nuclear antigen (PCNA) (14,27–30).

Human PCNA is a homotrimeric protein that encircles the duplex DNA forming a ring-shaped clamp and functions as a processivity factor for replicative DNA polymerases such as Polδ (31,32). Each of the three subunits is composed of two structurally similar domains, A and B, that are connected via an interdomain connector loop (12). In addition to being an essential component of the DNA replication machinery, PCNA also plays a role in cell cycle regulation (primarily in S-phase), translesion synthesis, long-patch BER and recombination (23,32). Because of its wide variety of roles, a number of PCNA-interacting proteins have been identified. Several of these partners contain a highly conserved PCNA-binding motif, QXXh[ILM]XXaa[FY] (where h (hydrophobic) is either Ile, Leu or Met and a (aromatic) is either Phe or Tyr, and X is any residue), referred to as a PCNA interacting protein (PIP) box (33,34). Most PCNA interacting partners contain at least one PIP box, while others contain as many as three PIP boxes as seen in the case of Pol η (35). NEIL1 also interacts with PCNA, but does not possess a conserved PIP-box motif. Instead, the interaction domain on NEIL1 was previously mapped to residues 289–311 located in the disordered C-terminal region of the enzyme (27).

In the studies presented here, we characterized the complex formed between NEIL1 and PCNA using size exclusion chromatography (SEC), native gel electrophoresis, atomic force microscopy (AFM) and small angle X-ray scattering (SAXS). SEC analysis suggested that the sizes of the NEIL1-PCNA and NEIL1-DNA-PCNA complexes were not large enough to account for homotrimeric PCNA bound to one or multiple molecules of NEIL1. AFM and SAXS measurements confirmed this observation indicating that PCNA no longer forms the typical ring-like structure in the presence of NEIL1.

MATERIALS AND METHODS

Overexpression and purification of constructs of NEIL1 and PCNA

The full-length genomic human NEIL1 (with a lysine at position 242) construct was cloned and purified as described previously (36,37); this is thus the unedited version of the NEIL1 enzyme (38). C-terminal truncation constructs of NEIL1, Δ56, Δ78 and Δ100 were either previously expressed and purified (36) or synthesized by Genscript and sub-cloned into a pET30a vector for expression. All NEIL1 constructs were expressed in Rosetta2 (DE3) pLysS *Escherichia coli* cells (Novagen), followed by isopropyl-β-D-thiogalactopyranoside induction either for 4 h at 30°C or overnight at 12–16°C. The cell pellets were resuspended in a buffer containing 50 mM sodium phosphate, pH 7.5, 150 mM NaCl, 10 mM imidazole, 10% (v/v) glycerol, 5 mM β-Me and 1 mM PMSF and sonicated. Clarified cell lysates were added to pre-equilibrated TALON cobalt resin (Clontech). The proteins were eluted using 250 mM imidazole in the above buffer and applied over a HiTrap SP-FF column (GE healthcare). A linear NaCl gradient (from 300 mM–1 M) was used to elute the enzymes and the resultant fractions were pooled, concentrated and applied over a Superdex 200

size exclusion column (GE Healthcare) in a buffer containing 20 mM Tris-HCl, pH 7.5, 300 mM NaCl, 10% (v/v) glycerol and 1 mM dithiothreitol (DTT). Fractions were pooled, concentrated and flash-frozen aliquots were stored at −80°C.

A pET11-a plasmid containing the gene for human PCNA (a kind gift from Dr Todd Washington, University of Iowa, USA) was transformed into Rosetta2-DE3-pLysS cells for protein expression. A single colony was picked and inoculated in 1 l of LB medium. Upon reaching log phase, cells were induced with 1 mM isopropyl-β-D-thiogalactopyranoside and harvested after 3 h at 37°C. Pelleted cells were lysed in a buffer containing 25 mM HEPES, pH 7.5, 300 mM NaCl and 5 mM imidazole, supplemented with 2 mM DNAse and 1 mM PMSF. Cell lysates were clarified at 13 000 rpm for 45 min at 4°C. The supernatant was applied over a .22 μm filter and loaded onto a chelating column charged with 100 mM nickel sulfate (GE Healthcare). A linear gradient from 5–500 mM imidazole was used to elute bound PCNA. Fractions containing PCNA were pooled and buffer exchanged into 25 mM HEPES, pH 7.5, 100 mM NaCl and 1 mM DTT. The protein was then loaded onto a DEAE column and eluted using a gradient of NaCl (100–1000 mM). Peak fractions were pooled and concentrated down to less ~1 ml to inject onto a Superdex 200 size exclusion column (GE healthcare) in a buffer containing 10 mM HEPES, pH 7.5 and 100 mM NaCl. Fractions were pooled, concentrated and flash frozen for long-term storage at −80°C.

DNA oligonucleotides, complex formation and gel filtration

Oligonucleotides (15-mer) containing an uncleavable abasic site analog, tetrahydrofuran (THF) and complementary strands were purchased from Midland Certified Reagent Co. (Midland, TX, USA) and purified by urea polyacrylamide gel electrophoresis. Upon annealing the two strands oligonucleotides containing either a 5-mer bubble or duplex DNA with C opposite the THF moiety were obtained (Figure 1C).

NEIL1-DNA complexes were prepared by combining NEIL1 and DNA (either bubble or duplex) in a buffer containing 10 mM HEPES, pH 7.5, 100 mM NaCl and 1 mM DTT in a 1:1 molar ratio. Complexes were incubated on ice for 30 min prior to SEC analysis. For NEIL1-DNA-PCNA complex, a 1:1 molar ratio of NEIL1 and DNA was incubated on ice for 30 min prior to the addition of the PCNA trimer such that the final ratio of NEIL1:DNA:PCNA was 3:3:1. The complex of both proteins and DNA was further incubated for 30 min on ice prior to gel-filtration analysis. SEC was performed using a Superdex 200 column in a buffer containing 10 mM HEPES, 100 mM NaCl and 1 mM DTT. The column was calibrated using blue dextran (to determine the void volume) and three standards of known molecular weights and Stoke's radii, ferritin (61 Å), aldolase (48.1 Å) and myoglobin (19 Å).

Far-Western analysis and cell culture

Samples for far-Western analysis were boiled in sodium dodecyl sulphate (SDS)-sample buffer and loaded on a 4–12%
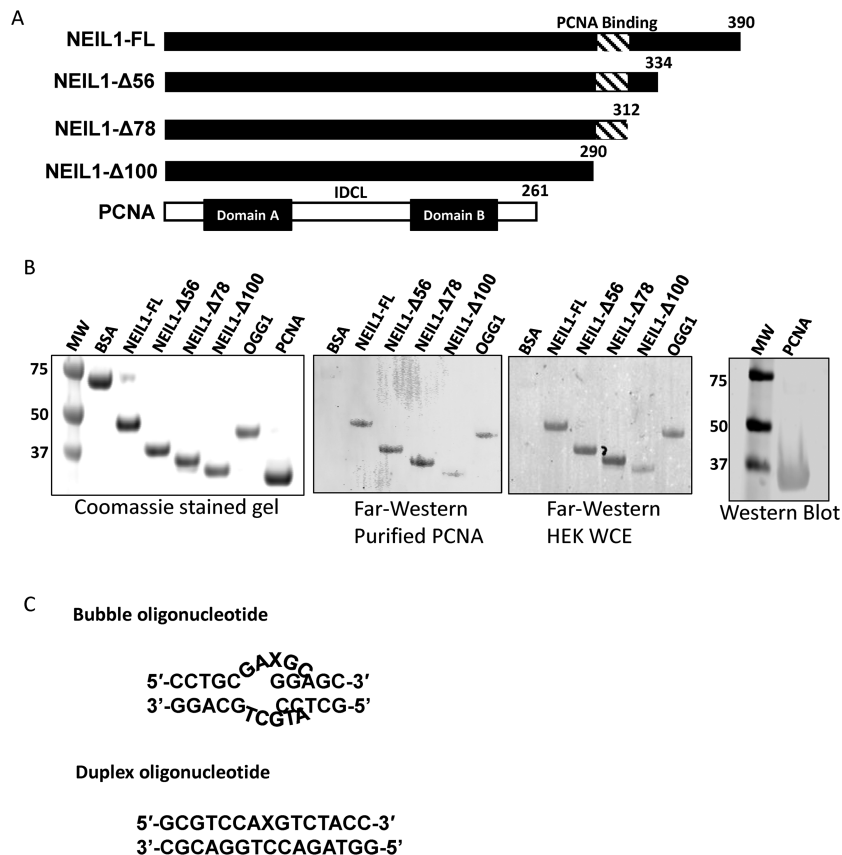
Figure 1. NEIL1 and proliferating cell nuclear antigen (PCNA) constructs and complex formation. (**A**) Domain organization of full-length (FL) and C-terminal truncation constructs of the NEIL1 DNA glycosylase and PCNA. (**B**) Far-Western analysis indicating complex formation between NEIL1 and PCNA. *Left panel*, sodium dodecyl sulphate-polyacrylamide gel electrophoresis Coomassie stained gel indicating the position of 50 pmol of bovine serum albumin (negative control), all constructs of NEIL1, OGG1 (positive control) and PCNA. *Middle panels*, far-Western analysis where bovine serum albumin, NEIL1 constructs and OGG1 were transferred to a nitrocellulose membrane, denatured on the membrane, renatured slowly, incubated with either purified PCNA (10 pmol/ml) or HEK293 whole cell extract (WCE), and probed with an anti-PCNA antibody to detect an interaction. *Right panel*, Western blot analysis of purified PCNA (control). (**C**) Sequences of the oligonucleotides used to study NEIL1-DNA-PCNA complexes. The X represents non-cleavable tetrahydrofuran, an abasic site analog.

precast gel (Novex) and run for 1 h at a constant 180 V. The gel was transferred to an Immobilon®-FL PVDF membrane (Millipore). The membrane was washed (2X for 10 min each) with 1X phosphate buffered saline (PBS) and 1 mM DTT. The membrane was then incubated in PBS with 6 M guanidine-HCl and 1 mM DTT for 30 min at room temperature with gentle shaking. The proteins on the membrane were then gradually refolded using serial dilutions of guanidine-HCl (in PBS with 1 mM DTT) to a final concentration of 0.09 M guanidine-HCL (6 M, 3 M, 1.5 M, 0.75 M, 0.375 M, 0.1875 M and 0.09 M). The first 5 steps were performed at room temperature for 30 min. The penultimate and ultimate steps were performed at 4°C. The membranes were then blocked for 1 h using PBS blocking reagent (LI-COR biosciences) and further incubated with a pre-prepared HEK293T cell lysate (1 mg/ml in Cell Lytic M buffer, Sigma) or purified protein, overnight. The membranes were then washed (3X) with cold PBS containing 0.05% Tween-20 and then processed using a standard Western blot protocol (LI-COR Biosciences). Anti-PCNA monoclonal antibody (PC-10, SC-56 purchased from Santa Cruz Biotechnology, Lot #

D1613) was diluted 1:200 in blocking reagent. The blot was then incubated with goat anti-mouse secondary antibody (LI-COR biosciences, IRDye 800CW, Lot # C40213-01) and scanned using an Odyssey CLx imaging system (LI-COR biosciences). The HEK293T cells used to generate lysates for the far-Western analysis were cultured in Dulbecco's modified Eagle's medium supplemented with 10% fetal bovine serum and 1% penicillin–streptomycin. To prepare cell lysates, cells were scraped into PBS, washed in cold PBS and lysed cell lytic M reagent (Sigma) supplemented with a protease inhibitor cocktail (Roche).

Native agarose gel electrophoresis and mass spectrometry (MS) analysis

A horizontal 0.8% agarose gel (~3 mm thick) was prepared in a buffer containing 25 mM Tris-HCl (pH 8.5) and 19.2 mM glycine. The comb was placed in the center of the gel. NEIL1 and PCNA at 0.5–2 mg/ml or individual fractions obtained from the gel filtration analysis were added to 2X sample buffer (20% glycerol and 0.2% bromophenol blue) and loaded on the gel. The gel was run at 50 V for 1 h at room temperature and stained with Coomassie blue. Pro-

teins with a pI > pH of the gel migrate toward the cathode while proteins with a pI < pH migrate toward the anode. Individual bands containing either protein alone or a protein complex were excised from the gel and were prepared for mass spectrometry (MS) analysis using standard tryptic digest procedures (39). Gel lanes were cut into 1 mm³ pieces and destained with 50 mM ammonium bicarbonate in 50% acetonitrile. Protein samples were reduced by the addition of 10 mM DTT at 55°C for 1 h and alkylated with 55 mM iodoacetamide. The gel pieces were then washed/rehydrated and dehydrated with 100 mM ammonium bicarbonate and 100% acetonitrile, respectively. The gel pieces were dried in a SpeedVac (Scientific Support, Hayward, CA, USA) and digestion was carried out for 18 h at 37°C with 7 ng/μl of trypsin. The tryptic peptides were acidified with 5% formic acid to stop the reaction, and dried in a SpeedVac (Scientific Support, Hayward, CA, USA). The dried peptide samples were re-suspended in a solution of 2.5% acetonitrile and 2.5% formic acid and loaded onto a 100 μm × 120 mm capillary column packed with MAGIC C18 (Michrom Biosources, CA, USA). Peptides were separated by a gradient of 5–35% acetonitrile and 0.1% formic acid for 30 min, 40–100% acetonitrile and 0.1% formic acid for 2 min, and 100% acetonitrile for 10 min. LC-MS based protein identification was performed on a linear ion trap (LTQ)-Orbitrap Discovery mass spectrometer coupled to a Surveyor MS Pump Plus (Thermo Fisher Scientific, Waltham, MA, USA). Separated peptides were introduced into the linear ion trap via a nanospray ionization source. Singly charged ions were excluded for MS/MS. Product ion spectra were searched using the SEQUEST search engine on Proteome Discoverer 1.4 (Thermo Fisher Scientific, MA, USA) against a curated human database with sequences in forward and reverse orientations. The database was indexed to allow for full trypsin enzymatic activity, two missed cleavages and peptides between the MW of 350–5000 Da. Search parameters set the mass tolerance at 20 ppm for precursor ions and 0.8 Da for fragment ions, dynamic modifications on methionine (+15.9949 Da: oxidation) and static modification on cysteine (+57.0215 Da: carbamidomethylation). The result files were then searched against the Scaffold software 4.3 (Proteome Software, OR, USA). Cross-correlation (Xcorr) significance filters were applied to limit the false positive rates to less than 1% in all data sets. The Xcorr values were as follows: (+1): 1.8, (+2): 2.15, (+3): 2.85, (+4): 3.25. The MS data obtained here for the purposes of protein identification are described in the Supplementary Data accompanying this paper.

Atomic force microscopy (AFM)

Samples were diluted to a concentration of 0.18 mg/ml in a buffer containing 25 mM HEPES, pH 7.5, 100 mM NaCl and 1 mM DTT. Diluted samples (∼7 μl) were deposited on freshly cleaved mica chips mounted to microscope slides. Samples were incubated for 5 min at room temperature. After incubation, slides were dipped in distilled water and allowed to air-dry overnight. Atomic force microscopy was performed with an Asylum Research MFP-3D-BIO (Asylum Research, an Oxford Instruments company; Santa Barbara, CA, USA). Images were acquired in

AC mode in air, using a 160 μm rectangular silicon probe with an aluminum reflex coating, tip radius of 9 ± 2 nm and a spring constant of 42 N/m (Olympus, AC160TS). Instrument settings were as follows: set point ∼600 mV, integral gain 4.5, drive amplitude 153 mV, drive frequency 73 KHz at a 90° scan angle, scan rate of 1 Hz, 512 lines per image and constant image gains. Topographical dimensions of sample features were analyzed off-line using Igor Pro 6.34 software (WaveMetrics, Portland, OR, USA).

Small angle X-ray scattering (SAXS)

SAXS data were collected at beamline 18-ID of the advanced photon source (APS) at Argonne National Laboratory for NEIL1 and at the SIBYLS beamline of the advanced light source (ALS) at Lawrence Berkeley National Laboratory for PCNA, NEIL1-DNA$_{duplex}$, and the NEIL1-DNA$_{duplex}$-PCNA complex (40). X-ray scattering data for NEIL1 was recorded with a MAR 165 detector (Rayonix) and 14 sequential exposures of 0.6 s each, at three concentrations (0.5, 1 and 2 mg/ml) up to a momentum transfer of 0.35 Å^{-1}. For PCNA, NEIL1-DNA$_{duplex}$ and the NEIL1-DNA$_{duplex}$-PCNA complex, scattering was recorded with a PILATUS detector (Dectris) at concentrations ranging from 1–6 mg/ml by measuring 24 sequential exposures at 0.2 s each up to a momentum transfer of 0.5 Å^{-1}. Concentrations were determined based on extinction coefficients and MW for individual proteins and using a Bradford assay for the complexes. Radial scattering measurements from each exposure were integrated followed by averaging of the exposures without any radiation damage. Averaged scattering curves from these exposures were buffer subtracted, concentration normalized and superimposed to evaluate concentration dependency using PRIMUS (41). Guinier approximation based forward scattering (I_0) and radius of gyration (R_g) were determined using PRIMUS and compared with corresponding values obtained by Gnom analysis (42). Scattering curves were further analyzed using ATSAS program for the calculation of distance distribution P(r), maximum dimension (Dmax), porod volume (V_ρ) and excluded volume (V_e). Calibrated forward scattering $I(0)$ from PCNA as well as SAXSMoW (43) were used for molecular weight estimation of individual scatterers. Three-dimensional shapes were reconstructed by 10 iterations of *ab initio* modeling using either GASBOR (44) or DAMMIN (45) followed by averaging of models using DAMAVER (46). SAXS models were deposited to the SASBDB database with the following codes: SASDBC7, human NEIL1; SASDBD7, human PCNA; SASDBB7, NEIL1-DNA$_{duplex}$ complex; SASDBA7, NEIL1-DNA$_{duplex}$-PCNA complex.

RESULTS

NEIL1 and PCNA form a complex in the presence and absence of DNA

Based on deletion analysis and structural studies, the C-terminal tail of NEIL1 comprising residues 290–390 is disordered and it is with this region that NEIL1 makes most of its protein–protein contacts (47,48). In order to confirm the interaction between NEIL1 and PCNA, we ex-

Table 1. Stokes radius obtained via SEC

Protein/Complex	MW (kDa)	Peak elution (ml)	Stokes radius (Å)
PCNA	89	13.5	42.6
NEIL1 alone	44.75	13.876	40
NEIL1-Δ100	34	15.7	28.37
NEIL1-PCNA		13.8	40.5
NEIL1-PCNA-Bubble		13.798	40.5
NEIL1-PCNA-Duplex		14.1	38.5

pressed and purified histidine-tagged full-length NEIL1 (NEIL1-FL) and C-terminal truncation constructs NEIL1-Δ56, NEIL1-Δ78 and NEIL1-Δ100 where the C-terminal 56, 78 and 100 residues were deleted, respectively (Figure 1A). We performed far-Western analysis where the NEIL1 constructs were transferred to a nitrocellulose membrane after sodium dodecyl sulphate-polyacrylamide gel electrophoresis (SDS-PAGE) and refolded prior to incubation with either HEK293T whole cell extracts or purified PCNA (Figure 1B). The blot was then probed with a PCNA antibody. Not surprisingly, NEIL1-FL, NEIL1-Δ56 and NEIL1-Δ78 that retain the intact PCNA interacting residues, displayed a positive interaction with PCNA. Non-specific, residual binding of NEIL1-Δ100 with PCNA present in whole cell extracts was observed but little to no binding was seen with purified PCNA. These data mimic those obtained previously where GST-tagged constructs of NEIL1 were used to map the interaction with PCNA (27). In the same study, PCNA was seen to enhance NEIL1's activity on single-stranded, fork and bubble substrates (27). Therefore, we further characterized the interaction between PCNA and NEIL1 in the presence and absence of DNA using bubble (DNA_{bubble}) and duplex (DNA_{duplex}) oligonucleotides containing the abasic site analog, THF (Figure 1C).

Our initial studies utilized SEC as a first step in isolating a complex of NEIL1 and PCNA. This was performed using a calibrated Superdex 200 column (GE Healthcare) with a separation range of 10 000–600 000 Da. Homotrimeric PCNA elutes at a Stokes radius of 42.6 Å, which corresponds to a ∼90 kDa protein (Table 1). Apo NEIL1 (44.75 kDa) elutes at Stokes radius of 40 Å and NEIL1-Δ100, which is ∼34 kDa size elutes at 15.8 ml and a Stokes radius of 28.4 Å (Supplementary Figure S1, Table 1). NEIL1 and PCNA were mixed in varying molar ratios of NEIL1:PCNA (1:1, 2:1 and 3:1, Supplementary Figure S2). All resulting complexes eluted as a single peak and increasing the amount of NEIL1 only caused an increase in absorbance height (mAU) but not in the Stokes radius. The Stokes radius for the highest molar ratio (3:1) was 40.5 Å (Figure 2A, Table 1). SDS-PAGE analysis of fractions from the eluted peak indicated the presence of both PCNA and NEIL1 in the individual fractions (Figure 2A, bottom). As expected, the NEIL1-Δ100 construct lacking the putative PCNA interacting region did not form a complex with PCNA in the absence or presence of DNA, and eluted as a separate peak on the gel filtration column (Figure 2A, Supplementary Figure S3A). Next, we preincubated NEIL1 with either DNA_{bubble} or DNA_{duplex} for 30 min in a 1:1 molar ratio followed by the addition of PCNA trimer such that the final ratio of NEIL1:DNA:PCNA trimer was 3:3:1.

SEC analysis followed by SDS-PAGE of the eluting complexes was performed. For the DNA_{bubble} oligonucleotide, a DNA-only peak with a high absorbance reading at 260 nm was observed (Figure 2B). This finding could be the result of either reduced affinity of NEIL1 for the bubble structure leading to an unbound fraction of the substrate or the result of partial melting of bubble oligonucleotide into ssDNA. As a control, NEIL1, NEIL1-Δ100 and PCNA were individually incubated with DNA_{bubble} and applied over the Superdex 200 column and the elution profiles reveal a large UV absorbance peak that corresponds to the DNA alone (Supplementary Figure S4). SEC analysis was also performed with the NEIL1-DNA_{duplex}-PCNA complex (Supplementary Figure S5). The Stokes radii for the complexes of NEIL1-DNA_{bubble}-PCNA and NEIL1-DNA_{duplex}-PCNA were 40.5 and 38.5 Å, respectively (Table 1, Figure 2B and C). The NEIL1-PCNA complexes appear to be smaller than what would be predicted for NEIL1 bound to trimeric PCNA, in the presence or absence of DNA. As a comparison, SEC data obtained for the PCNA-FEN1 complex and the PCNA-MutSα complex revealed the formation of much larger complexes (49,50). Overall, the data from the SEC analysis indicate that NEIL1 and PCNA form a complex either in the absence or presence of DNA, but the sizes of the eluting complexes suggest that the PCNA present in a complex with NEIL1 ± DNA may no longer be a homotrimer.

In order to confirm that NEIL1 and PCNA form a complex *in vitro*, we performed native agarose gel electrophoresis (51). An agarose gel (pH 8) was cast with the wells in the middle of the gel so that proteins with an isoelectric point (pI) higher than the pH of the gel and running buffer migrate toward the cathode while proteins with a low pI migrate toward the anode (Figure 2C and Supplementary Figure S3B). As such, NEIL1, which has a theoretical pI ∼9.4 migrates toward the cathode whereas PCNA, which has a low pI ∼4.5, migrates toward the anode (Figure 2C, lanes 1 and 2, respectively). Complexes of NEIL1-DNA_{bubble} and NEIL1-DNA_{duplex} were also analyzed using native gel electrophoresis (Figure 2C, lanes 3 and 4). The complex formed between NEIL1 and DNA_{bubble} migrated similarly to NEIL1 alone despite the negative charge imparted by the DNA whereas the NEIL1-DNA_{duplex} complex was seen to migrate toward the anode. The differences observed between the duplex and bubble DNA oligonucleotides can be attributed to the stability of the duplex over the bubble DNA. The complexes of PCNA and NEIL1 in the presence and absence of DNA complex migrated slightly toward the anode, but not as far into the gel as PCNA alone (Figure 2C, lanes 5–7), indicative of complex formation. In order to confirm that both NEIL1 and PCNA
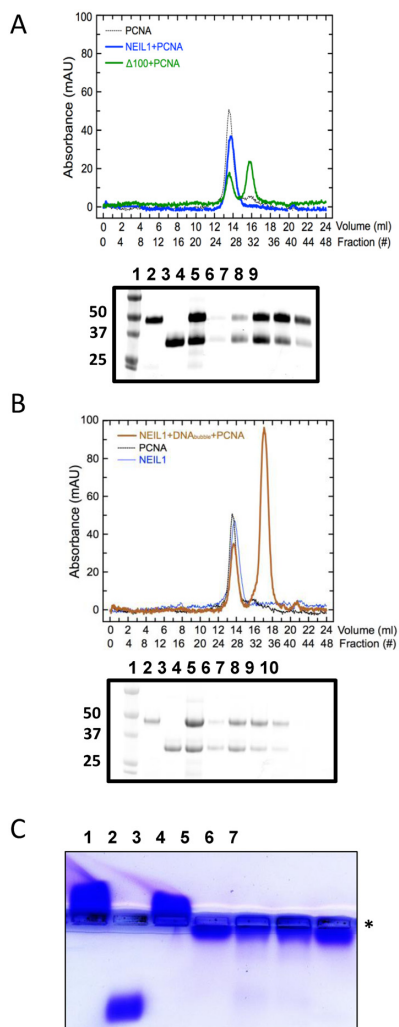
Figure 2. PCNA and NEIL1-FL can form a complex in the absence and presence of DNA. (**A**) Complex of PCNA and NEIL1 in the absence of DNA. *Top*, tracing from Superdex 200 size exclusion chromatography (SEC) column where a complex of NEIL1 and PCNA (3:1 molar ratio) is shown as a blue line, PCNA alone is shown as a black dotted line, and a NEIL1-Δ100-PCNA mixture is shown in green. NEIL1-Δ100 does not form a complex with PCNA and elutes separately from PCNA. *Bottom*, Coomassie stained gel of the fractions obtained after analysis by gel filtration. Lane 1, marker; lane 2, NEIL1-FL; lane 3, PCNA; lane 4, NEIL1-PCNA complex input prior to gel filtration; lane 5–9, fractions 25–29 (that correspond to 12.5–14.5 in ml as 0.5 ml fractions were collected for all samples) obtained after gel filtration, respectively. (**B**) Complex of PCNA and NEIL1 in the presence of DNA$_{bubble}$. *Top*, tracing from Superdex 200 column where a complex of NEIL1 and DNA$_{bubble}$ was preformed on ice (1:1 molar ratio) followed by the addition of PCNA such that NEIL1 and DNA were present in 3-fold excess over the PCNA trimer (solid brown line). PCNA and NEIL1 alone are shown as a black and blue dotted lines, respectively. Since 0.5 ml fractions were collected during SEC, corresponding fraction numbers are listed for clarity. *Bottom*, Coomassie stained gel of the fractions obtained after analysis by gel filtration. Lane 1, marker; lane 2, NEIL1-FL; lane 3, PCNA; lane 4, NEIL1-DNA$_{bubble}$-PCNA complex input prior to gel filtration; lanes 5–8, fractions 26–29 or 13–14.5 ml (0.5 ml fractions collected); lanes 9–10, fraction 33–34 obtained after gel filtration, respectively. (**C**) Native agarose gel electrophoresis: lane 1, 50 μM full-length NEIL1; lane 2, 50 μM PCNA; lane 3, NEIL1-DNA$_{bubble}$; lane 4, NEIL1-DNA$_{duplex}$; lane 5, NEIL1-PCNA; lane 6, NEIL1-DNA$_{bubble}$-PCNA; lane 7, NEIL1-DNA$_{duplex}$-PCNA. * indicates the location of the wells. Proteins with an isoelectric point (pI) higher than buffer pH migrate upward toward the cathode and those with a lower pI migrate downward toward the anode.

are present in the complexes, bands were excised from the gel, digested with trypsin and analyzed by MS. MS analysis identified the presence of both NEIL1 and PCNA in the complexes (Supplementary Figures S6 and S7). These data confirm that NEIL1 and PCNA form a stable complex *in vitro* both in the presence and absence of DNA.

## Analysis of the complex formed between NEIL1 and PCNA using AFM

We used AFM to gain further insight into the complex formed between NEIL1 and PCNA. Individual proteins or complexes that eluted after SEC were spotted onto mica disks and representative AFM images are displayed in Figure 3. Due to tip convolution, lateral AFM measurements are exaggerated in the XY dimension and were not utilized (52), however, accompanying height measurements for each sample were determined and are displayed below each image. The ring-shaped PCNA trimer ($\sim$90 kDa) is clearly visible in our analysis (Figure 3A top) with a measured height of $\sim$4 nm (Figure 3A bottom). These measurements are consistent with the crystal structure of PCNA where the trimer measures $\sim$8 nm in diameter and $\sim$3–4 nm in height (32). Previous AFM analysis performed with PCNA also indicated the presence of similar ring-shaped structures (53). We performed AFM analysis with NEIL1 alone (Figure 3B) and NEIL1 in a complex with either DNA$_{bubble}$ (Figure 3C) or DNA$_{duplex}$ (Figure 3D). Not surprisingly, the height measurements for apo NEIL1 and the NEIL1-DNA complexes were much smaller in comparison to the PCNA trimer. We then performed AFM analysis of the complexes formed between PCNA-NEIL1 in the absence and presence of DNA (Figure 3E–G). The complexes obtained did not reveal the presence of ring-shaped structures and height measurements from up to 10 independent fields were recorded for each sample and plotted as described previously in the form of a box plot (Figure 3H) (54). The height measurements for NEIL1-DNA-PCNA complexes appear to be similar to or smaller than trimeric PCNA alone. Taken together the AFM data concur with the data obtained from SEC and indicate that PCNA no longer forms a homotrimeric ring in the presence of NEIL1 and DNA.

Small-angle X-ray scattering analysis of NEIL1, PCNA and the NEIL1-PCNA-DNA complex

Since SAXS has been employed successfully to characterize proteins with flexible domains, we used this solution scattering method to gain structural insights into the NEIL1-DNA and NEIL1-DNA-PCNA assemblies (55). We obtained data for the NEIL1 and PCNA proteins alone to provide a necessary benchmark to scrutinize the complexes formed between NEIL1, DNA and PCNA. For each protein or complex studied, a relative plot of scattered intensities was plotted against momentum transfer and a characteristic pattern unique to each scatterer was observed (Figure 4A, Supplementary Figure S8). SAXS data were obtained for unliganded NEIL1 at three different concentrations (0.5–2 mg/ml). The linearity of the Guinier regions (56) indicates no aggregation and the curves superimpose across the concentration range suggesting no concentration dependency (Supplementary Figure S8A). Guinier
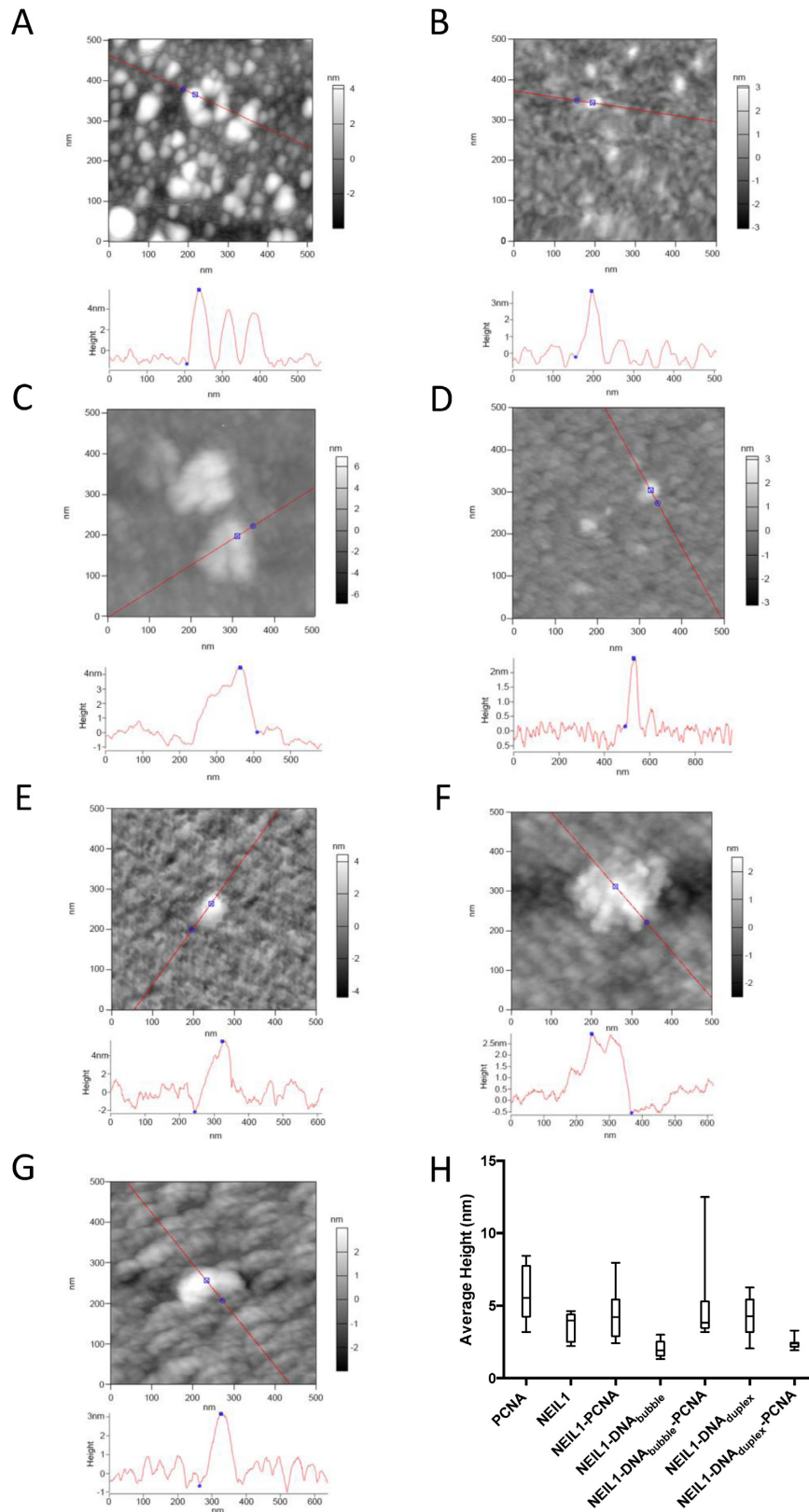
Figure 3. Atomic force microscopy (AFM) analysis of PCNA, NEIL1 and complexes in the absence and presence of DNA. (**A**) PCNA. (**B**) NEIL1. (**C**) NEIL1-PCNA. (**D**) NEIL1-DNA$_{bubble}$. (**E**) NEIL1-DNA$_{bubble}$-PCNA. (**F**) NEIL1-DNA$_{duplex}$. (**G**) NEIL1-DNA$_{duplex}$-PCNA. (**H**) Box plot comparing height measurements of parts A–G.
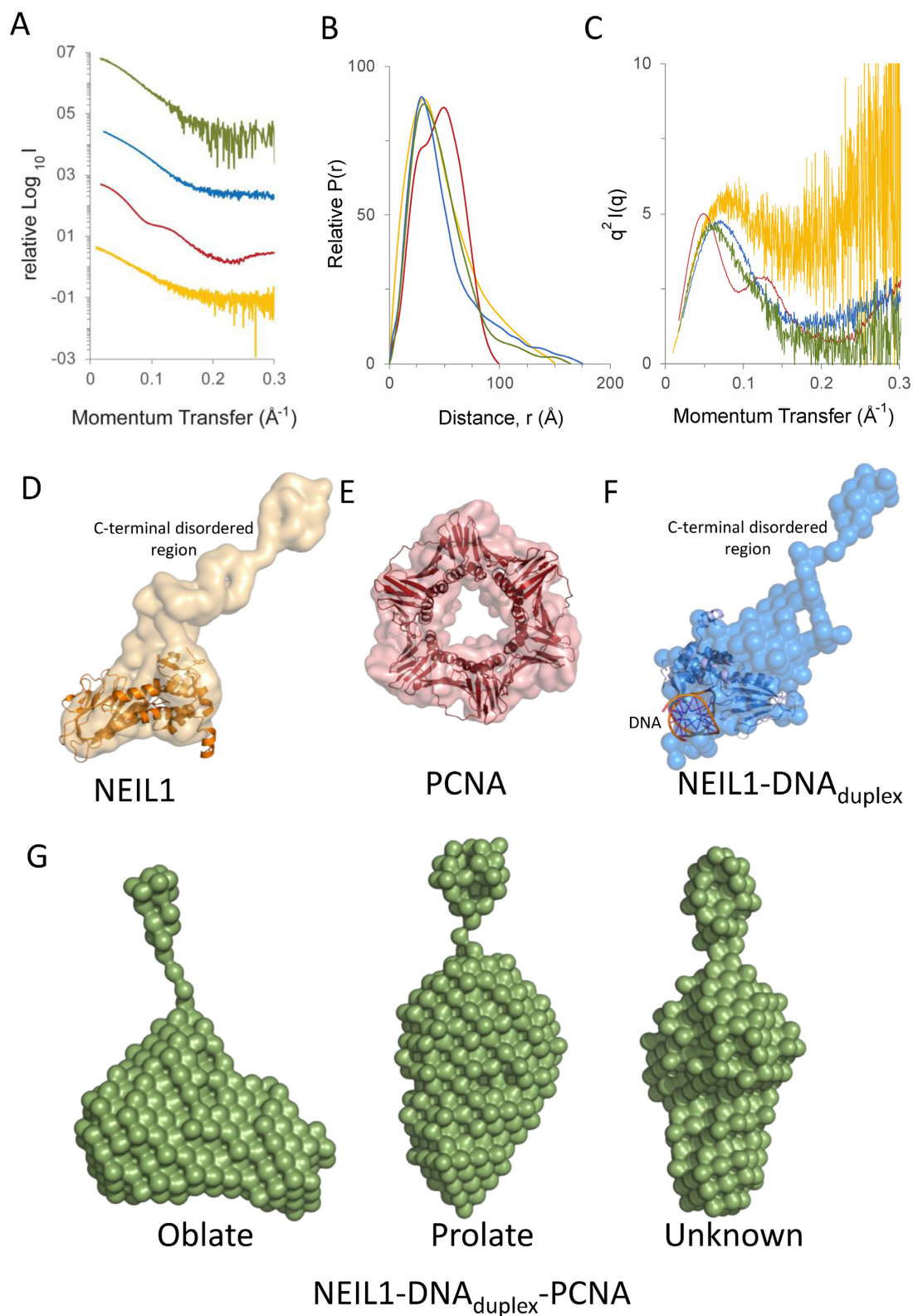
Figure 4. Small angle X-ray scattering (SAXS) analysis of PCNA, NEIL1, NEIL1-DNA and the NEIL1-DNA-PCNA complex. (**A**) Scattering intensity curves for NEIL1 (yellow), PCNA (red), NEIL1-DNA$_{duplex}$ (blue) and NEIL1-DNA$_{duplex}$-PCNA (green). The same color scheme is used throughout the figure. (**B**) Normalized pairwise interatomic distance distribution P[r] function for all proteins and complexes. (**C**) Kratky analysis indicating the degree of disorder of all proteins and complexes. (**D**) *Ab initio* shape reconstructed for NEIL1 generated in GASBOR indicates a compact core consistent with the crystal structure of NEIL1 (PDB ID, 1TDH (47)) and an extended region representing the disordered C-terminal tail. This result is consistent with NEIL1 model reported earlier (57). (**E**) *Ab initio* model of PCNA generated using GASBOR indicates a ring-shaped molecule that aligns well with the crystal structure of PCNA (PDB ID 1W60 (63)). (**F**) *Ab initio* model of the NEIL1-DNA$_{duplex}$ (PDB ID 1TDH (64)) generated using DAMMIN. (**G**) *Ab initio* models of the NEIL1-DNA$_{duplex}$-PCNA complex generated in DAMMIN using asymmetry settings of oblate, prolate and unknown.

and gnom-based analysis for NEIL1 indicate that the enzyme is a monomer in solution with R_g and D_{max} values (Table 2) similar to those published previously (57). For PCNA, a concentration series of 2–6 mg/ml was collected and the data reveal no aggregation as indicated by the linearity of the Guinier plot (Supplementary Figure S8). The plot of intensity (*I*) versus momentum transfer (*s*) produced curves with two signature inflection points (Figure 4A, Supplementary Figure S8), a feature that was previously observed with archaeal PCNA from *Sulfolobus sulfataricus* and *Thermococcus kodakarensis* (58–60). Notably, this feature is present in the scattering curves of trimeric, ring-shaped PCNA and its complexes with DNA ligase (59), NucS (61), MutSα (50) and Msh6 (62) where binding to the respective partners does not cause disassembly of PCNA trimer. However, the two characteristic inflection points are not present when PCNA no longer forms ring and is present as a monomer, as seen in the case of mutant PCNA or in the TIP-PCNA complex (58).

We used the DNA_{duplex} oligonucleotide in all SAXS experiments owing to its stability over the bubble-containing DNA. NEIL1 formed a complex with DNA_{duplex} and the estimated molecular weight suggested a stoichiometry of 1:1 $NEIL1:DNA_{duplex}$ in solution (Table 2). Data collected for the NEIL1-DNA_{duplex} complex at three different concentrations (1.3–2.1 mg/ml) aligned well, indicating no concentration dependency and the linearity within the Guinier region indicated no aggregation (Supplementary Figure S8C). SAXS data obtained for the NEIL1-DNA_{duplex}-PCNA complex (concentrations ranging from 0.6–2.8 mg/ml) indicate that the shape of the scattering curve is different than the shape of the curve for PCNA alone (Figure 4A) and lacks the characteristic two inflection points. This provides for a qualitative means to address the disassembly of the PCNA trimer upon interaction with NEIL1 and DNA_{duplex}. Furthermore, analysis of the NEIL1-DNA_{duplex}-PCNA complex using SAXSMoW based molecular weight estimation (Table 2) (43) at the lowest concentration (0.6 mg/ml or ∼7 nM), indicates formation of a 1:1:1 complex of NEIL1:DNA:PCNA(monomer). An overlay of the scattering data obtained for the NEIL1-DNA_{duplex}-PCNA complex at all concentrations indicate concentration dependency in the Guinier region (Supplementary Figure S8D). We observed a consistent increase in the radius of gyration, forward scattering $I(0)$ and SAXSMoW-based molecular weight with increasing concentrations, which suggests the potential for concentration-dependent oligomerization of this complex (Supplementary Table S1). These data suggest that the NEIL1-mediated disruption of PCNA trimer could be a transient interaction with PCNA in equilibrium between trimeric and monomeric states.

Pairwise distance distribution function, *P(r)*, analysis provides further insight into the size and overall shape of the proteins and complexes analyzed by SAXS (Figure 4B). Gnom-based maximum dimension (Dmax) (42) calculations suggested sizes of 150 Å and 97.2 Å for NEIL1 and PCNA respectively (Table 2). These calculated Dmax values are similar to those reported earlier for both NEIL1 and PCNA (55,57). The distance distribution plot for PCNA (Figure 4B, red) shows a pattern consistent with that observed previously (50,59,61). P(r) analysis of the complexes

reveals Dmax values of 175 Å and 164 Å for the NEIL1-DNA_{duplex} and the NEIL1-DNA_{duplex}-PCNA complexes, respectively (Table 2, and Figure 4B). The distance distribution plot for the NEIL1-DNA_{duplex}-PCNA complex (Figure 4B, green) is most similar to the plot for unliganded NEIL1 (Figure 4B, yellow), suggesting an elongated shape for the complex.

It is well established that NEIL1 has a disordered C-terminal tail between residues 290 and 390 and this partial disorder is reflected in the Kratky plot, which indicates a curve that is initially parabolic in nature but trends upwards at higher angles indicative of partial disorder (>0.15 Å^{-1} Figure 4C, yellow) (30,47,55,57). For PCNA on the other hand, a relatively ordered protein, the shape of the Kratky plot is characteristic of a globular protein and possesses two inflection points (Figure 4C, red) (55,60). Kratky analysis of the NEIL1-DNA_{duplex} and NEIL1-DNA_{duplex}-PCNA complexes reveal a parabolic curve much like unliganded NEIL1, but do not possess the elevated baseline at the higher angles (Figure 4C, green and blue lines). Taken together, these data indicate that the disordered tail of NEIL1 assumes a more ordered architecture mediated by interactions with DNA and PCNA.

Ab initio shape reconstruction of NEIL1 using GASBOR (44) generated a model (Figure 4D, Table 2) with a compact globular domain and a long tubular unstructured region. The SAXS data and the model presented here for NEIL1 are in agreement with data obtained previously (57). A cartoon representation of the crystal structure of NEIL1 (PDB ID 1TDH (47)) was manually fitted into the ordered globular domain of the envelope generated from GASBOR (Figure 4D). PCNA data (at a concentration of 6 mg/ml) produced a hollow ring-like *ab initio* model using GASBOR (Figure 4E, Table 2). This model is similar to that obtained previously (55) and the crystal structure (PDB ID 1W60 (63)) was manually fitted to the model (Figure 4E). The *ab initio* shape reconstruction using DAMMIN (45) for the NEIL1-DNA_{duplex} complex at a concentration of 1.9 mg/ml indicated an extra scattering mass between the N- and C-terminal domains of NEIL1 (Figure 4F, Table 2). Based on crystal structures of several members of the Fpg/Nei DNA glycosylase family bound to DNA, the DNA binding region lies orthogonal to the long axis of the protein in the cleft between the N- and C-terminal domains of the enzymes (12). The crystal structure of unliganded NEIL1 (PDB 1TDH) was superimposed with the crystal structure of its viral ortholog bound to DNA (MvNei1, PDB ID 3VK7 (64)). Human NEIL1 with the DNA from MvNei1 were modeled into the SAXS envelope (Figure 4F). *Ab initio* modeling of the solution structure of the NEIL1-DNA_{duplex}-PCNA assembly produced an ensemble of three potential shapes when different particle anisometry parameters (oblate, prolate and unknown) were used in DAMMIN (Figure 4G, Table 2). The models obtained here do not possess a hollow ring as seen with the models obtained for the PCNA-MutSα (50) and PCNA-Lig complexes (59) where PCNA remains intact. The three models combined with the scattering data, SAXSMoW-based molecular weight assessments and distance distribution plots support the idea that PCNA in a complex with NEIL1-DNA_{duplex} is no longer ring-shaped.

Table 2. SAXS data collection parameters

Data collection parameters	NEIL1	PCNA	NEIL1-DNA$_{duplex}$	NEIL1-DNA$_{duplex}$-PCNA
Beamline	APS	ALS	ALS	ALS
Detector	MAR	PILATUS	PILATUS	PILATUS
Wavelength (Å)	1.033	1.127	1.127	1.127
Q Range (Å^{-1})	0.005–0.328	0.016–0.0528	0.016–0.528	0.016–0.528
Exposure time (s)	8.4 (14 × 0.6)	4.8 (24 × 0.2)	4.8 (24 × 0.2)	4.8 (24 × 0.2)
Concentration (mg/ml)	0.5–2	1–6	1.3–2.1	0.6–2.8
Temperature (°C)	10	10	10	10
Structural parameters				
$I(0)/c$ from Guinier	4.4 ± 0.03	483.2 ± 1.4	309.0 ± 2.09	707.9 ± 7.04
R_g (Å) from Guinier	35.5 ± 3.31	34.4 ± 0.25	33.0 ± 1.78	34.0 ± 0.77
$I(0)/c$ from $P(r)$	4.1	486.2	337	733
R_g (Å) from $P(r)$	38.3	34.4	41	37.8
D_{max} (Å)	150	97.2	175	164
Porod volume (Å^3)	81 372	128 204	92 043	113 195
Molecular weight determination (kDa)				
MW$_{SAXSMoW}$	65.5	85.9	63.9	86.7
MW$_{I(0)/C}$	48.1	—	61.5	133.8
Expected theoretical	44.8	89.1	55.8	85.5
Modeling parameters				
Symmetry	P1	P3	P1	P1
Particle anisometry	Unknown	Oblate	Unknown	Oblate (O) Prolate (P) Unknown (U)
# of modeling iterations	10	10	10	10
X^2 of the model with lowest NSD	1.1	0.8	0.5	0.5 (O) 0.5 (P) 0.5 (U)
DAMAVER NSD (var)	1.4 ± 0.08	1.1 ± 0.08	0.7 ± 0.04	0.5 ± 0.03 (O) 0.5 ± 0.05 (P) 0.5 ± 0.09 (U)
Modeling tool	GASBOR	GASBOR	DAMMIN	DAMMIN

DISCUSSION

Processivity clamps are present in all three domains of life and play a critical role in several facets of DNA metabolism including replication, recombination and repair (65–67). Although there is little sequence homology among PCNA molecules from bacteria, archaea and eukarya, they are all ring-shaped with similar overall structural features, encircle duplex DNA and serve as platforms for the binding numerous replication and repair factors (31,32). The bacterial sliding clamp also called the β-clamp is a homodimer where each subunit comprises three domains thereby forming a ring with pseudo 6-fold symmetry (68). The archaeal sliding clamps are more versatile: for example, PCNA from *Sulfolobus sulfataricus* is a heterotrimer in which each subunit is able to bind to different proteins thereby facilitating diversity in the number of interacting partners, whereas the genome of the archaeal species *Thermococcus kodakarensis* encodes for 2 PCNA genes, PCNA1 and PCNA2, both of which form homotrimers (69–71). Human PCNA is encoded by a single gene and forms a homotrimer where each subunit is identical and comprised of two structurally similar domains (72). Replication, transcription and repair are tightly regulated processes and crosstalk between DNA repair enzymes and PCNA is therefore necessary and inevitable.

Since the first crystal structure of eukaryotic PCNA was solved in 1994, numerous structures of either post-translationally modified PCNA (by ubiquitination, sumoylation, etc.), or PCNA in a complex with peptides and full-length interacting partners have been studied (32,73). To

date, almost 100 structures of PCNA from various species have been deposited in the PDB. As such, the mechanism of recruitment of replication and repair factors mediated by interactions with PCNA, has been brought to light. Most proteins bind to PCNA via a conserved PIP motif, which has evolved subtle differences in the conserved sequence allowing for variability in the binding affinities of partners thereby enabling the recruitment of specific proteins to DNA (35). An example of sequence variability in the PIP motif is seen in the translesion polymerases η, ι and κ that lack a conserved glutamine residue that replicative polymerase such as polymerase delta use to bind tightly to PCNA (74). The crystal structure of PCNA bound to full-length FEN1 reveals 3 molecules of FEN1 bound to each monomer of PCNA where each FEN1 molecule makes slightly different contacts with PCNA (75). It is also apparent from this structure that the network of interactions between FEN1 and PCNA extends beyond the PIP motif where the core domain of FEN1 forms secondary contacts with PCNA. While the PIP motif is absolutely essential for some proteins to interact with PCNA, not all PCNA interacting partners possess this conserved motif as seen in the case of NEIL1 (27).

Regulation of PCNA function by its binding partners has been documented previously. For example, in the archaeal species *T. kodakarensis*, a small protein named the Thermococcales inhibitor of PCNA (or TIP) lacks a canonical PIP-motif yet binds to PCNA1 and prevents trimer formation (76). The crystal structure of the PCNA-TIP complex was recently solved and sheds light on the mechanism by which

TIP accomplishes the disruption of the PCNA trimer (58). TIP binds to PCNA within the same region as FEN1 and other PCNA interacting partners, but causes rearrangement of the interdomain connector loop and induces a conformational change between the two structurally similar domains of PCNA that results in an unfavorable interface for trimer formation (58). Another example where PCNA function is inhibited is by the cell-cycle regulator p21 (77). However, instead of disrupting trimer formation, p21 binds tightly to PCNA and prevents other proteins such as FEN1, replication factor C or polδ from interacting with it (72,78,79). Other ways by which the PCNA trimer can be destabilized without intervention from other protein binding partners *in vitro* include, either the presence of 50% glycerol or as little as 10% polyethylene glycol as well as the use of ammonium sulfate precipitation methods during the purification step (80). Disruption of PCNA can also occur as a consequence of mutation in critical subunit interface residues. In yeast, mutation of two conserved residues E113 and G178 to glycine and serine, respectively, caused disruption of the PCNA trimer by altering the inter-subunit interface and resulting in the inhibition of translesion synthesis by DNA polymerases η and δ (81).

In this report, we explored the effects of binding of the NEIL1 DNA glycosylase to PCNA. We isolated a complex of NEIL1 and PCNA in the absence and presence of DNA using SEC. Height measurements obtained from AFM analysis indicated that PCNA does not exist as a ring-shaped trimer in the presence of NEIL1. In order to confirm this observation we performed SAXS analysis with the individual proteins and complexes with DNA. The scattering curve for the NEIL1-DNA-PCNA complex lacked the scattering features seen with PCNA alone. Previous SAXS analyses obtained for the PCNA-FEN1 and PCNA-MutSα complexes indicate that PCNA retains its ring-like nature as noted in the scattering data and seen with *ab initio* models obtained (50,58). In contrast, our SAXS data mimic the scattering data obtained for the PCNA-TIP complex where the presence of TIP disrupts clamp formation (58). Taken together the data presented here indicate that the PCNA present in the NEIL1-DNA-PCNA complex is no longer ring-shaped and could represent a mechanistic switch from replication to BER where replication is stalled by disruption of the PCNA trimer, thereby allowing for repair to occur. Whether this is a feature unique to the NEIL1 DNA glycosylase remains to be elucidated.

Interactions between PCNA and its interacting partners may be far more complex than initially conceived. The homotrimeric nature of this protein may be disrupted either by other proteins such as NEIL1 or by mutant forms of PCNA in the cell that can prevent stable trimer formation. Chemical denaturation and NMR-based studies comparing the backbone dynamics of human and yeast PCNA suggest that human PCNA is less stable than its yeast counterpart (82). In summary, it appears that human PCNA is more pliable than initially conceived and can form a continuum of structures in the cell ranging from monomers and trimers to double trimers depending on a functional requirement. Furthermore, regulation of PCNA activity by various post translational modifications and their effects on mediating protein–protein interactions with repair enzymes such as NEIL1, still remains to be elucidated (83).

SUPPLEMENTARY DATA

Supplementary Data are available at NAR Online.

REFERENCES

1. De Bont,R. and van Larebeke,N. (2004) Endogenous DNA damage in humans: a review of quantitative data. *Mutagenesis*, **19**, 169–185.
2. Cooke,M.S., Evans,M.D., Dizdaroglu,M. and Lunec,J. (2003) Oxidative DNA damage: mechanisms, mutation, and disease. *FASEB J.*, **17**, 1195–1214.

3. Martin,L.J. (2008) DNA damage and repair: relevance to mechanisms of neurodegeneration. *J. Neuropathol. Exp. Neurol.*, **67**, 377–387.

4. Cadet,J., Douki,T. and Ravanat,J.L. (2011) Measurement of oxidatively generated base damage in cellular DNA. *Mutat. Res.*, **711**, 3–12.

5. Wallace,S.S. (2014) Base excision repair: a critical player in many games. *DNA Repair (Amst)*, **19**, 14–26.

6. Lindahl,T. and Barnes,D.E. (2000) Repair of endogenous DNA damage. *Cold Spring Harb. Symp. Quant. Biol.*, **65**, 127–133.

7. Reik,W. (2007) Stability and flexibility of epigenetic gene regulation in mammalian development. *Nature*, **447**, 425–432.

8. Bauer,N.C., Corbett,A.H. and Doetsch,P.W. (2015) The current state of eukaryotic DNA base damage and repair. *Nucleic Acids Res.*, **43**, 10083–10101.

9. David,S.S., O'Shea,V.L. and Kundu,S. (2007) Base-excision repair of oxidative DNA damage. *Nature*, **447**, 941–950.

10. Krokan,H.E. and Bjørås,M. (2013) Base excision repair. *Cold Spring Harb. Perspect. Biol.*, **5**, a012583.

11. Brooks,S.C., Adhikary,S., Rubinson,E.H. and Eichman,B.F. (2013) Recent advances in the structural mechanisms of DNA glycosylases. *Biochim. Biophys. Acta*, **1834**, 247–271.

12. Prakash,A., Doublié,S. and Wallace,S.S. (2012) The Fpg/Nei family of DNA glycosylases: substrates, structures, and search for damage. *Prog. Mol. Biol. Transl. Sci.*, **110**, 71–91.

13. Jacobs,A.L. and Schar,P. (2012) DNA glycosylases: in DNA repair and beyond. *Chromosoma*, **121**, 1–20.

14. Wallace,S.S. (2013) DNA glycosylases search for and remove oxidized DNA bases. *Environ. Mol. Mutagen.*, **54**, 691–704.

15. Hegde,M.L., Hazra,T.K. and Mitra,S. (2008) Early steps in the DNA base excision/single-strand interruption repair pathway in mammalian cells. *Cell Res.*, **18**, 27–47.

16. Krishnamurthy,N., Zhao,X., Burrows,C.J. and David,S.S. (2008) Superior removal of hydantoin lesions relative to other oxidized bases by the human DNA glycosylase hNEIL1. *Biochemistry*, **47**, 7137–7146.

17. Zhou,J., Fleming,A.M., Averill,A.M., Burrows,C.J. and Wallace,S.S. (2015) The NEIL glycosylases remove oxidized guanine lesions from telomeric and promoter quadruplex DNA structures. *Nucleic Acids Res.*, **43**, 4039–4054.

18. Krokeide,S.Z., Laerdahl,J.K., Salah,M., Luna,L., Cederkvist,F.H., Fleming,A.M., Burrows,C.J., Dalhus,B. and Bjørås,M. (2013) Human NEIL3 is mainly a monofunctional DNA glycosylase removing spiroimindiohydantoin and guanidinohydantoin. *DNA Repair (Amst)*, **12**, 1159–1164.

19. Hailer,M.K., Slade,P.G., Martin,B.D., Rosenquist,T.A. and Sugden,K.D. (2005) Recognition of the oxidized lesions spiroiminodihydantoin and guanidinohydantoin in DNA by the mammalian base excision repair glycosylases NEIL1 and NEIL2. *DNA Repair (Amst)*, **4**, 41–50.

20. Dou,H., Mitra,S. and Hazra,T.K. (2003) Repair of oxidized bases in DNA bubble structures by human DNA glycosylases NEIL1 and NEIL2. *J. Biol. Chem.*, **278**, 49679–49684.

21. Zhao,X., Krishnamurthy,N., Burrows,C.J. and David,S.S. (2010) Mutation versus repair: NEIL1 removal of hydantoin lesions in single-stranded, bulge, bubble, and duplex DNA contexts. *Biochemistry*, **49**, 1658–1666.

22. Neurauter,C.G., Luna,L. and Bjørås,M. (2012) Release from quiescence stimulates the expression of human NEIL3 under the control of the Ras dependent ERK-MAP kinase pathway. *DNA Repair (Amst)*, **11**, 401–409.

23. Mjelle,R., Hegre,S.A., Aas,P.A., Slupphaug,G., Drablos,F., Saetrom,P. and Krokan,H.E. (2015) Cell cycle regulation of human DNA repair and chromatin remodeling genes. *DNA Repair (Amst)*, **30**, 53–67.

24. Liu,M., Doublié,S. and Wallace,S.S. (2013) Neil3, the final frontier for the DNA glycosylases that recognize oxidative damage. *Mutat. Res.*, **743–744**, 4–11.

25. Hegde,M.L., Hegde,P.M., Bellot,L.J., Mandal,S.M., Hazra,T.K., Li,G.M., Boldogh,I., Tomkinson,A.E. and Mitra,S. (2013) Prereplicative repair of oxidized bases in the human genome is mediated by NEIL1 DNA glycosylase together with replication proteins. *Proc. Natl. Acad. Sci. U.S.A.*, **110**, E3090–E3099.

26. Hazra,T.K., Izumi,T., Boldogh,I., Imhoff,B., Kow,Y.W., Jaruga,P., Dizdaroglu,M. and Mitra,S. (2002) Identification and characterization of a human DNA glycosylase for repair of modified bases in oxidatively damaged DNA. *Proc. Natl. Acad. Sci. U.S.A.*, **99**, 3523–3528.

27. Dou,H., Theriot,C.A., Das,A., Hegde,M.L., Matsumoto,Y., Boldogh,I., Hazra,T.K., Bhakat,K.K. and Mitra,S. (2008) Interaction of the human DNA glycosylase NEIL1 with proliferating cell nuclear antigen. The potential for replication-associated repair of oxidized bases in mammalian genomes. *J. Biol. Chem.*, **283**, 3130–3140.

28. Hegde,M.L., Theriot,C.A., Das,A., Hegde,P.M., Guo,Z., Gary,R.K., Hazra,T.K., Shen,B. and Mitra,S. (2008) Physical and functional interaction between human oxidized base-specific DNA glycosylase NEIL1 and flap endonuclease 1. *J. Biol. Chem.*, **283**, 27028–27037.

29. Theriot,C.A., Hegde,M.L., Hazra,T.K. and Mitra,S. (2010) RPA physically interacts with the human DNA glycosylase NEIL1 to regulate excision of oxidative DNA base damage in primer-template structures. *DNA Repair (Amst)*, **9**, 643–652.

30. Hegde,P.M., Dutta,A., Sengupta,S., Mitra,J., Adhikari,S., Tomkinson,A.E., Li,G.M., Boldogh,I., Hazra,T.K., Mitra,S. *et al.* (2015) The C-terminal domain (CTD) of human DNA glycosylase NEIL1 is required for forming BERosome repair complex with DNA replication proteins at the replicating genome: dominant negative function of the CTD. *J. Biol. Chem.*, **290**, 20919–20933.

31. De Biasio,A. and Blanco,F.J. (2013) Proliferating cell nuclear antigen structure and interactions: too many partners for one dancer? *Adv. Protein Chem. Struct. Biol.*, **91**, 1–36.

32. Dieckman,L.M., Freudenthal,B.D. and Washington,M.T. (2012) PCNA structure and function: insights from structures of PCNA complexes and post-translationally modified PCNA. *Subcell Biochem.*, **62**, 281–299.

33. Tsurimoto,T. (1999) PCNA binding proteins. *Front. Biosci.*, **4**, D849–D858.

34. Warbrick,E. (1998) PCNA binding through a conserved motif. *Bioessays*, **20**, 195–199.

35. Masuda,Y., Kanao,R., Kaji,K., Ohmori,H., Hanaoka,F. and Masutani,C. (2015) Different types of interaction between PCNA and PIP boxes contribute to distinct cellular functions of Y-family DNA polymerases. *Nucleic Acids Res.*, **43**, 7898–7910.

36. Bandaru,V., Cooper,W., Wallace,S.S. and Doublié,S. (2004) Overproduction, crystallization and preliminary crystallographic analysis of a novel human DNA-repair enzyme that recognizes oxidative DNA damage. *Acta Crystallogr. D Biol. Crystallogr.*, **60**, 1142–1144.

37. Prakash,A., Carroll,B.L., Sweasy,J.B., Wallace,S.S. and Doublié,S. (2014) Genome and cancer single nucleotide polymorphisms of the human NEIL1 DNA glycosylase: activity, structure, and the effect of editing. *DNA Repair (Amst)*, **14**, 17–26.

38. Yeo,J., Goodman,R.A., Schirle,N.T., David,S.S. and Beal,P.A. (2010) RNA editing changes the lesion specificity for the DNA repair enzyme NEIL1. *Proc. Natl. Acad. Sci. U.S.A.*, **107**, 20715–20719.

39. Tacoma,R., Fields,J., Ebenstein,D.B., Lam,Y.W. and Greenwood,S.L. (2016) Characterization of the bovine milk proteome in early-lactation Holstein and Jersey breeds of dairy cows. *J. Proteomics*, **130**, 200–210.

40. Classen,S., Hura,G.L., Holton,J.M., Rambo,R.P., Rodic,I., McGuire,P.J., Dyer,K., Hammel,M., Meigs,G., Frankel,K.A. *et al.* (2013) Implementation and performance of SIBYLS: a dual endstation small-angle X-ray scattering and macromolecular crystallography beamline at the Advanced Light Source. *J. Appl. Crystallogr.*, **46**, 1–13.

41. Konarev,P.V., Volkov,V.V., Sokolova,A.V., Koch,M.H.J. and Svergun,D.I. (2003) PRIMUS: a Windows PC-based system for small-angle scattering data analysis. *J. Appl. Crystallogr.*, **36**, 1277–1282.

42. Svergun,D.I. (1992) Determination of the regularization parameter in indirect-transform methods using perceptual criteria. . *J. Appl. Crystallogr.*, **25**, 495–503.

43. Fischer,H., de Oliveira Neto,M., Napolitano,H.B., Polikarpov,I. and Craievich,A.F. (2010) Determination of the molecular weight of proteinsin solution from a single small-angle X-rayscattering measurement on a relative scale. *J. Appl. Crystallogr.*, **43**, 101–109.

44. Svergun,D.I., Petoukhov,M.V. and Koch,M.H. (2001) Determination of domain structure of proteins from X-ray solution scattering. *Biophys. J.*, **80**, 2946–2953.

45. Svergun,D.I. (1999) Restoring low resolution structure of biological macromolecules from solution scattering using simulated annealing. *Biophys. J.*, **76**, 2879–2886.

46. Volkov,V.V. and Svergun,D.I. (2003) Uniqueness of ab initio shape determination in small-angle scattering. *J. Appl. Crystallogr.*, **36**, 860–864.

47. Doublié,S., Bandaru,V., Bond,J.P. and Wallace,S.S. (2004) The crystal structure of human endonuclease VIII-like 1 (NEIL1) reveals a zincless finger motif required for glycosylase activity. *Proc. Natl. Acad. Sci. U.S.A.*, **101**, 10284–10289.

48. Hegde,M.L., Hegde,P.M., Arijit,D., Boldogh,I. and Mitra,S. (2012) Human DNA glycosylase NEIL1's interactions with downstream repair proteins is critical for efficient repair of oxidized DNA base damage and enhanced cell survival. *Biomolecules*, **2**, 564–578.

49. Sakurai,S., Kitano,K., Okada,K., Hamada,K., Morioka,H. and Hakoshima,T. (2003) Preparation and crystallization of human flap endonuclease FEN-1 in complex with proliferating-cell nuclear antigen, PCNA. *Acta Crystallogr. D Biol. Crystallogr.*, **59**, 933–935.

50. Iyer,R.R., Pohlhaus,T.J., Chen,S., Hura,G.L., Dzantiev,L., Beese,L.S. and Modrich,P. (2008) The MutSalpha-proliferating cell nuclear antigen interaction in human DNA mismatch repair. *J. Biol. Chem.*, **283**, 13310–13319.

51. Kim,R. (2011) Native agarose gel electrophoresis of multiprotein complexes. *Cold Spring Harb. Protoc.*, **2011**, 884–887.

52. Taatjes,D.J., Quinn,A.S., Lewis,M.R. and Bovill,E.G. (1999) Quality assessment of atomic force microscopy probes by scanning electron microscopy: correlation of tip structure with rendered images. *Microsc. Res. Tech.*, **44**, 312–326.

53. Shiomi,Y., Usukura,J., Masamura,Y., Takeyasu,K., Nakayama,Y., Obuse,C., Yoshikawa,H. and Tsurimoto,T. (2000) ATP-dependent structural change of the eukaryotic clamp-loader protein, replication factor C. *Proc. Natl. Acad. Sci. U.S.A.*, **97**, 14127–14132.

54. Krzywinski,M. and Altman,N. (2014) Visualizing samples with box plots. *Nat. Methods*, **11**, 119–120.

55. Tsutakawa,S.E., Hura,G.L., Frankel,K.A., Cooper,P.K. and Tainer,J.A. (2007) Structural analysis of flexible proteins in solution by small angle X-ray scattering combined with crystallography. *J. Struct. Biol.*, **158**, 214–223.

56. Guinier,A. (1939) La diffraction des rayons X aux tres petits angles; application a l'etude de phenomenes ultramicroscopiques. *Ann. Phys. (Paris)*, **12**, 161–237.

57. Hegde,M.L., Tsutakawa,S.E., Hegde,P.M., Holthauzen,L.M., Li,J., Oezguen,N., Hilser,V.J., Tainer,J.A. and Mitra,S. (2013) The disordered C-terminal domain of human DNA glycosylase NEIL1 contributes to its stability via intramolecular interactions. *J. Mol. Biol.*, **425**, 2359–2371.

58. Altieri,A.S., Ladner,J.E., Li,Z., Robinson,H., Sallman,Z.F., Marino,J.P. and Kelman,Z. (2016) A small protein inhibits proliferating cell nuclear antigen by breaking the DNA clamp. *Nucleic Acids Res.*, **44**, 6232–6241.

59. Pascal,J.M., Tsodikov,O.V., Hura,G.L., Song,W., Cotner,E.A., Classen,S., Tomkinson,A.E., Tainer,J.A. and Ellenberger,T. (2006) A flexible interface between DNA ligase and PCNA supports conformational switching and efficient ligation of DNA. *Mol. Cell*, **24**, 279–291.

60. Putnam,C.D., Hammel,M., Hura,G.L. and Tainer,J.A. (2007) X-ray solution scattering (SAXS) combined with crystallography and computation: defining accurate macromolecular structures, conformations and assemblies in solution. *Q. Rev. Biophys.*, **40**, 191–285.

61. Creze,C., Ligabue,A., Laurent,S., Lestini,R., Laptenok,S.P., Khun,J., Vos,M.H., Czjzek,M., Myllykallio,H. and Flament,D. (2012) Modulation of the Pyrococcus abyssi NucS endonuclease activity by replication clamp at functional and structural levels. *J. Biol. Chem.*, **287**, 15648–15660.

62. Shell,S.S., Putnam,C.D. and Kolodner,R.D. (2007) The N terminus of Saccharomyces cerevisiae Msh6 is an unstructured tether to PCNA. *Mol. Cell*, **26**, 565–578.

63. Kontopidis,G., Wu,S.Y., Zheleva,D.I., Taylor,P., McInnes,C., Lane,D.P., Fischer,P.M. and Walkinshaw,M.D. (2005) Structural and biochemical studies of human proliferating cell nuclear antigen complexes provide a rationale for cyclin association and inhibitor design. *Proc. Natl. Acad. Sci. U.S.A.*, **102**, 1871–1876.

64. Imamura,K., Averill,A., Wallace,S.S. and Doublié,S. (2012) Structural characterization of viral ortholog of human DNA glycosylase NEIL1 bound to thymine glycol or 5-hydroxyuracil-containing DNA. *J. Biol. Chem.*, **287**, 4288–4298.

65. Prelich,G., Kostura,M., Marshak,D.R., Mathews,M.B. and Stillman,B. (1987) The cell-cycle regulated proliferating cell nuclear antigen is required for SV40 DNA replication in vitro. *Nature*, **326**, 471–475.

66. Hedglin,M., Kumar,R. and Benkovic,S.J. (2013) Replication clamps and clamp loaders. *Cold Spring Harb. Perspect. Biol.*, **5**, a010165.

67. Warbrick,E. (2000) The puzzle of PCNA's many partners. *Bioessays*, **22**, 997–1006.

68. Kong,X.P., Onrust,R., O'Donnell,M. and Kuriyan,J. (1992) Three-dimensional structure of the beta subunit of E. coli DNA polymerase III holoenzyme: a sliding DNA clamp. *Cell*, **69**, 425–437.

69. MacNeill,S.A. (2016) PCNA-binding proteins in the archaea: novel functionality beyond the conserved core. *Curr. Genet.*, **62**, 527–532.

70. Williams,G.J., Johnson,K., Rudolf,J., McMahon,S.A., Carter,L., Oke,M., Liu,H., Taylor,G.L., White,M.F. and Naismith,J.H. (2006) Structure of the heterotrimeric PCNA from Sulfolobus solfataricus. *Acta Crystallogr. Sect. F Struct. Biol. Cryst. Commun.*, **62**, 944–948.

71. Winter,J.A. and Bunting,K.A. (2012) Rings in the extreme: PCNA interactions and adaptations in the archaea. *Archaea*, 951010.

72. Gulbis,J.M., Kelman,Z., Hurwitz,J., O'Donnell,M. and Kuriyan,J. (1996) Structure of the C-terminal region of p21(WAF1/CIP1) complexed with human PCNA. *Cell*, **87**, 297–306.

73. Krishna,T.S., Kong,X.P., Gary,S., Burgers,P.M. and Kuriyan,J. (1994) Crystal structure of the eukaryotic DNA polymerase processivity factor PCNA. *Cell*, **79**, 1233–1243.

74. Hishiki,A., Hashimoto,H., Hanafusa,T., Kamei,K., Ohashi,E., Shimizu,T., Ohmori,H. and Sato,M. (2009) Structural basis for novel interactions between human translesion synthesis polymerases and proliferating cell nuclear antigen. *J. Biol. Chem.*, **284**, 10552–10560.

75. Sakurai,S., Kitano,K., Yamaguchi,H., Hamada,K., Okada,K., Fukuda,K., Uchida,M., Ohtsuka,E., Morioka,H. and Hakoshima,T. (2005) Structural basis for recruitment of human flap endonuclease 1 to PCNA. *EMBO J.*, **24**, 683–693.

76. Li,Z., Huang,R.Y., Yopp,D.C., Hileman,T.H., Santangelo,T.J., Hurwitz,J., Hudgens,J.W. and Kelman,Z. (2014) A novel mechanism for regulating the activity of proliferating cell nuclear antigen by a small protein. *Nucleic Acids Res.*, **42**, 5776–5789.

77. Chen,J., Peters,R., Saha,P., Lee,P., Theodoras,A., Pagano,M., Wagner,G. and Dutta,A. (1996) A 39 amino acid fragment of the cell cycle regulator p21 is sufficient to bind PCNA and partially inhibit DNA replication in vivo. *Nucleic Acids Res.*, **24**, 1727–1733.

78. Maga,G. and Hubscher,U. (2003) Proliferating cell nuclear antigen (PCNA): a dancer with many partners. *J. Cell Sci.*, **116**, 3051–3060.

79. Waga,S., Hannon,G.J., Beach,D. and Stillman,B. (1994) The p21 inhibitor of cyclin-dependent kinases controls DNA replication by interaction with PCNA. *Nature*, **369**, 574–578.

80. Naryzhny,S.N., Desouza,L.V., Siu,K.W. and Lee,H. (2006) Characterization of the human proliferating cell nuclear antigen physico-chemical properties: aspects of double trimer stability. *Biochem. Cell Biol.*, **84**, 669–676.

81. Dieckman,L.M. and Washington,M.T. (2013) PCNA trimer instability inhibits translesion synthesis by DNA polymerase eta and by DNA polymerase delta. *DNA Repair (Amst)*, **12**, 367–376.

82. De Biasio,A., Sanchez,R., Prieto,J., Villate,M., Campos-Olivas,R. and Blanco,F.J. (2011) Reduced stability and increased dynamics in the human proliferating cell nuclear antigen (PCNA) relative to the yeast homolog. *PLoS One*, **6**, e16600.

83. Tsutakawa,S.E., Yan,C., Xu,X., Weinacht,C.P., Freudenthal,B.D., Yang,K., Zhuang,Z., Washington,M.T., Tainer,J.A. and Ivanov,I. (2015) Structurally distinct ubiquitin- and sumo-modified PCNA: implications for their distinct roles in the DNA damage response. *Structure*, **23**, 724–733.